

PAPERS

Optical phonon characteristics of an orthorhombic-transformed polymorph of CaTa_2O_6 single crystal fibre

To cite this article: R M Almeida *et al* 2014 *Mater. Res. Express* 1 016304

View the [article online](#) for updates and enhancements.

Related content

- [Single-crystal structure determination and infrared reflectivity study of the \$\text{Li}_2\text{CaHfF}_8\$ scheelite](#)
A P Ayala, C W A Paschoal, J-Y Gesland *et al.*
- [Optical phonon modes and infrared dielectric properties of monoclinic \$\text{CoWO}_4\$ microcrystals](#)
Roberto L Moreira, Rafael M Almeida, Kísla P F Siqueira *et al.*
- [Raman and infrared spectroscopy of \$\text{LaYbO}_3\$](#)
R L Moreira, A Feteira and A Dias

Recent citations

- [Optical phonon modes and infrared dielectric properties of monoclinic \$\text{CoWO}_4\$ microcrystals](#)
Roberto L Moreira *et al*



IOP | ebooks™

Bringing you innovative digital publishing with leading voices to create your essential collection of books in STEM research.

Start exploring the collection - download the first chapter of every title for free.

Optical phonon characteristics of an orthorhombic-transformed polymorph of CaTa_2O_6 single crystal fibre

R M Almeida¹, M R B Andreeta², A C Hernandez³, A Dias⁴ and R L Moreira¹

¹Departamento de Física, ICEX, Universidade Federal de Minas Gerais, C.P. 702, 30123-970, Belo Horizonte MG, Brazil

²Departamento de Engenharia de Materiais, Universidade Federal de São Carlos, C.P. 676, 13565-905, São Carlos SP, Brazil

³Instituto de Física de São Carlos, Universidade de São Paulo, C.P. 369, 13560-970, São Carlos SP, Brazil

⁴Departamento de Química, ICEB, Universidade Federal de Ouro Preto, 35400-000, Ouro Preto MG, Brazil

E-mail: bmoreira@fisica.ufmg.br

Received 18 December 2013, revised 30 January 2014

Accepted for publication 3 February 2014


Published 7 March 2014

Materials Research Express 1 (2014) 016304

doi:[10.1088/2053-1591/1/1/016304](https://doi.org/10.1088/2053-1591/1/1/016304)

Abstract

Infrared-reflectivity spectroscopy and micro-Raman scattering were used to determine the optical phonon features of orthorhombic calcium tantalite (CaTa_2O_6) single crystal fibres. The fibres, obtained by the Laser-Heated Pedestal Growth method, grew into an ordered cubic structure ($Pm\bar{3}$). Long-time annealing was used to induce a polymorphic transformation to an *aeschynite* orthorhombic structure ($Pnma$ space group). The phase transformation led to the appearance of structural domains and micro-cracks, responsible for diffuse scattering and depolarization of the scattered light in the visible range, but not in the infrared region. Thus, polarized infrared spectroscopy could be performed within oriented single domains, with an appropriate microscope, allowing us to determine all relevant polar phonons of the orthorhombic CaTa_2O_6 . The obtained phononic dielectric response, $\langle \epsilon_r \rangle = 22.4$ and $\langle Q_u \times f \rangle = 86 \times 10^3$ GHz, shows the appropriateness of the material for microwave applications. Totally symmetric Raman modes could be resolved by polarization, after re-polishing the cracked sample surface.

 Online supplementary data available from stacks.iop.org/MRX/1/016304/mmedia

Keywords: polymorphism, infrared spectroscopy, Raman scattering, CaTa_2O_6 , polar phonons

1. Introduction

In recent years, calcium tantalite (CaTa_2O_6) has attracted particular attention; it has been considered for microwave and optical applications, when prepared in ceramic or crystal forms, respectively [1–5]. At room temperature, this material can present different polymorphic phases depending on the sample preparation conditions [6–8], which determine, as usual, the physical properties of the system. Therefore, in order to describe the physical behavior of the material, comprehensive studies must be carried out within its different polymorphic phases.

In a previous work, we have investigated the optical vibrational properties of a CaTa_2O_6 single crystal fibre grown by the Laser-Heated Pedestal Growth method (LHPG) [9]. The samples obtained by this method always crystallize within an ordered cubic structure belonging to the $Pm\bar{3}$ space group [10]. This effect has been attributed to the fast cooling rate inherent to the LHPG method. Indeed, this structural phase is metastable, and, by an appropriate thermal treatment, it can be transformed into an orthorhombic phase of the *aeschynite* group ($Pnma$ structure) [11], which is stable down to room temperature. This orthorhombic phase can also be obtained directly during the sample growth, by slow crystallization at temperatures above 700 °C [1, 2, 7]. A third and less common room temperature polymorph with a cubic structure has also been cited. It is a calcium-deficient simple perovskite ($Pm\bar{3}m$ space group), which could be obtained by low-temperature crystallization, i.e., below 700 °C [6, 7]. However, investigations of the physical properties of the material within this phase are still lacking. It is also worth mentioning that two high temperature polymorphs of CaTa_2O_6 , with tetragonal and cubic symmetries, have been reported above 1450 °C [12], although their structures have not been determined yet.

In view of the aforementioned microwave (MW) and optical applications, the knowledge of the optical phonon behavior is mandatory. Indeed, the intrinsic dielectric response of a dielectric material in the MW range is determined by the characteristics of its polar phonon modes (dielectric strengths and damping) [13]. In addition, rare-earth doped single crystal fibres of CaTa_2O_6 present strong infrared emission under light pumping [3, 5]—the phonon modes play an important role in the tuning conditions. Therefore, the investigation of the complete phonon spectra of CaTa_2O_6 in its different polymorphic phases contributes to the understanding of its dielectric behavior and optimization of the technical applications within the appropriate crystal phase. Concerning the ordered $Pm\bar{3}$ cubic phase, we have already reported a thorough Raman and infrared investigation of its optical vibrational modes, with a comprehensive set of phonon modes and their characteristics [9]. Very recently, we were able to obtain single crystal fibres of CaTa_2O_6 with the orthorhombic $Pnma$ structure, by long-time annealing (24 h) at 1200 °C [11]. The purpose of the present work is to investigate the Raman and infrared phonon modes of this centro-symmetrical structure. Despite the appearance of multiple domains, efforts have been made to obtain the correct symmetries of the phonons, particularly of the polar modes, by using microscopic techniques and different sample geometries. We were able to assign all the observed polar modes to their corresponding symmetries and to obtain the intrinsic dielectric response of the orthorhombic phase, which proved to be very adequate for

MW applications. In addition, the totally symmetric (Raman) modes could be experimentally discerned.

2. Experimental

CaTa₂O₆ single crystal fibres with average diameters of 400 μm and up to 20 mm length were prepared by the LHPG method, as described in detail in previous works [3–5, 9, 11]. In short, the starting reagents (CaCO₃ and Ta₂O₅) were ball milled for 24 h and used to prepare cylindrical pedestals (1.0 mm diameter, 50 mm long), which were melted by a CO₂ laser (Synrad-Evolution, 125 W, 10.6 μm) using the experimental setup described elsewhere [14, 15]. The fibres were optically transparent, free of cracks or striations, but contained small facets parallel to the cylindrical axis. Structural characterization of the as-grown fibres by single crystal x-ray diffraction (Gemini-Oxford diffractometer, Mo-Kα source, 45 kV, 40 mA) showed that they grew into a single $Pm\bar{3}$ ordered cubic phase, with a lattice parameter $a = 7.745 \text{ \AA}$ and $Z = 4$. The fibre's longitudinal axis was identified as nearly parallel to one of the cubic edges, and the small facets were observed to be mainly normal to the cubic [110] directions [9]. Thermal treatments to induce polymorphic transformation were done in air, at 1200 °C, for 24 h. The heating/cooling rates used were $\pm 5 \text{ }^\circ\text{C min}^{-1}$. In order to perform optical measurements, oriented samples were cut from the fibres (400 μm diameter × 800 μm length) and polished to an optical grade.

CaTa₂O₆ ceramics were prepared by the conventional solid-state route. Stoichiometric amounts of Ca(OH)₂ and Ta₂O₅ were mixed in an acetone medium and reacted at 1200 °C, for 4 h. The resulting powders were investigated by the x-ray diffraction technique (XRD) in a high resolution Shimadzu D-6000 diffractometer, with the following measuring parameters: 10–60° 2θ, 15 s/step of 0.02°2θ, 40 kV, and 20 mA (the angular range corresponds to CuKα radiation). The powder XRD of the ceramic sample, performed with a Bragg-Brentano configuration, showed a single phase, impurity free, *aeschnite* structure, belonging to the orthorhombic *Pnma* space group (#62), with unit cell parameters $a = 11.068 \text{ \AA}$, $b = 7.503 \text{ \AA}$, and $c = 5.373 \text{ \AA}$ (see figure S1 in the supplementary data, available at stacks.iop.org/MRX/1/016304/mmedia).

Polarized and unpolarized micro-Raman scattering spectra of the crystal fibres and ceramic samples were recorded at room temperature (295 K) using a Horiba/Jobin-Yvon LABRAM-HR spectrometer, equipped with a LN₂-cooled CCD detector and a confocal Olympus microscope (20 × objective). The spectral resolution was *ca.* 1 cm⁻¹ and the spatial resolution was 2 μm. The measurements were carried out in back-scattering geometry, using the 633 nm line of He-Ne laser (6 mW at the sample's surface) as the excitation source. Appropriate interference and edge filters, a half-wave plate and a polarizer were used. The spectra were obtained between 40 and 1100 cm⁻¹, by averaging 10 accumulations of 30 s, and were corrected for the Bose–Einstein thermal factor [16].

Polarized infrared measurements of the CaTa₂O₆ fibres were performed with a Fourier transform spectrometer (FTIR: Nicolet, Nexus 470), equipped with a modified Centaurus microscope (10 × magnification). This commercial instrument has been designed for the mid-infrared region (550–4000 cm⁻¹), where a SiC source, a KBr:Ge beamsplitter and a MCT detector, plus a grid polarizer on a ZnSe substrate constitute the standard accessories for building up the appropriate configuration. In order to reach the far-infrared region (50–700 cm⁻¹), we adapted the microscope to receive a Si-bolometer detector [17]. Then, far-infrared

measurements could be performed using the following configuration: SiC source, a solid-state Si beamsplitter, the Si-bolometer detector and a wire grid polarizer on a PE substrate. The reflectivity spectra in both spectral regions were obtained under nitrogen purge, by averaging 128 scans for each polarization direction (parallel to the principal axes of the crystal), with spectral resolution better than 4 cm^{-1} . Gold mirrors were used for the reference spectra. In order to observe single domains and avoid polarization leaks, the measuring regions on the sample were limited to $200\text{ }\mu\text{m} \times 200\text{ }\mu\text{m}$. The infrared reflectivity spectra obtained in mid- and far-infrared regions matched well in the superposition region (within 2%).

3. Results and discussions

The optically-active vibrational modes of CaTa_2O_6 crystal fibres crystallized within the ordered $Pm\bar{3}$ cubic structure were previously obtained by Raman and infrared spectroscopies [9, 11]. A total of 21 Raman-active modes at the Brillouin-zone centre ($5A_g \oplus 5E_g \oplus 11F_g$), along with their appropriate symmetries were discerned by special scattering configurations. In addition, 13 of the 16 predicted triply degenerate (F_u) infrared modes were obtained by micro-infrared reflectivity [9]. After long-time annealing, the Raman spectra became completely different, owing to the polymorphic transformation to an orthorhombic phase. Indeed, the fibre samples were no longer transparent, acquiring a whitish color, while their Raman spectra became stronger and lost all the polarization features—the spectra for different configurations are essentially equal, which makes it difficult to attribute the phonon features to their respective symmetries [11]. The orthorhombic structure of the transformed phase was confirmed by comparing the non-polarized Raman spectra of the annealed fibre with that of the CaTa_2O_6 ceramic (figure S2 of the supplementary data, available at stacks.iop.org/MRX/1/016304/mmedia, shows essentially the same Raman features for both samples). A representative set of the 54 predicted modes for the orthorhombic *aeschnite* structure has been discerned, although their symmetries were only tentatively attributed, after lattice dynamics calculations [11, 18].

The depolarization of the scattered light in the visible range, the enhancement of the inelastic scattering and the acquired whitish color are indicative of the appearance of multiple domains and micro-cracks (responsible for diffuse scattering). Therefore, in order to try to obtain polarization-resolved spectra we re-polished the fibre samples and looked for polarization features. Microphotographs of a fibre, before and after re-polishing, are shown in figure S3 of the supplementary data (available at stacks.iop.org/MRX/1/016304/mmedia).

Before presenting the experimental results, let us discuss the expected symmetries of the CaTa_2O_6 phonon modes in the *aeschnite* structure. In this structure, Ca ions occupy the Wyckoff $4c$ sites of C_s^{xz} symmetry; Ta ions are on the $8d$ sites of general C_1 symmetry; two oxygen ions sit on the $8d$ positions (C_1) and another two on the $4c$ sites (C_s^{xz}). Therefore, the corresponding decomposition in irreducible representations of the zone-centre modes [19] becomes $\Gamma = 15A_g (\text{R}) \oplus 12B_{1g} (\text{R}) \oplus 15B_{2g} (\text{R}) \oplus 12B_{3g} (\text{R}) \oplus 12A_u (\text{silent}) \oplus 14B_{1u} (\text{IR}) \oplus 11B_{2u} (\text{IR}) \oplus 14B_{3u} (\text{IR}) \oplus 1B_{1u} (\text{acoustic}) \oplus 1B_{2u} (\text{acoustic}) \oplus 1B_{3u} (\text{acoustic})$. Thus, a total of 54 Raman (R) and 39 infrared (IR) modes are expected for this structure.

Figure 1 presents the polarized room-temperature Raman spectra of the orthorhombic CaTa_2O_6 single crystal fibre (re-polished), with *parallel* (black) and *crossed* (red) lights. Although polarization features could be revealed by these spectra, we were unable to find a single domain signature, likely because the micro-cracks prevent us from eliminating diffuse

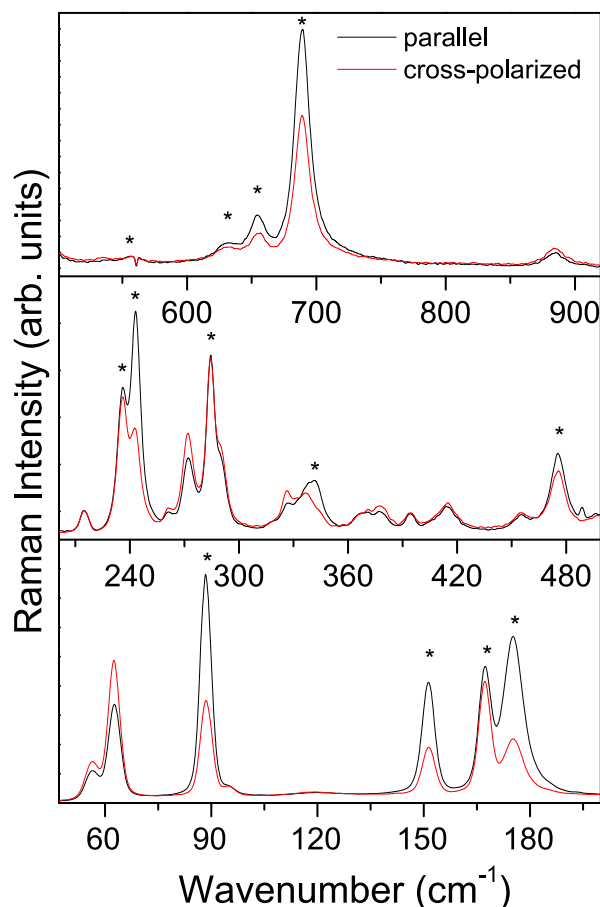


Figure 1. Polarized room-temperature Raman spectra of orthorhombic CaTa_2O_6 single crystal fibre with *parallel* (black) and *crossed* (red) lights. The revealed totally symmetric vibrational modes are indicated by asterisks.

scattering. Despite that, as shown in the figure, we could discern the totally symmetric A_g modes, which tend to be enhanced in parallel-polarized light (conversely to B_g -type modes, which are usually stronger in cross-polarized light). The experimentally revealed totally symmetric modes are indicated by asterisks in the figure.

As a whole, a total of 13 totally symmetric A_g -type modes could be experimentally resolved in our spectra. As already explained, we were unable to discern the different domains, and therefore, we could not separate the different B_g modes. Despite that, 17 B_g -type modes were unambiguously discerned in the polarized spectra of figure 1. A summary of the observed Raman modes and their attributed symmetries is presented in table 1.

Conversely to the Raman scattering spectra, polarized micro-infrared reflectivity showed strongly polarization-dependent spectra. We believe that in the larger wavelength range used in this second case (2.5 μm to 200 μm), diffuse scattering/reflection due to the micro-cracks is strongly reduced, in comparison to the visible range. Indeed, we were able to orient the sample under an infrared microscope, and even to find single-domains as large as 200 μm wide. Therefore, polarized infrared reflectivity spectra of the orthorhombic CaTa_2O_6 within particular single domains were performed, and the spectra attributed to their appropriate symmetries.

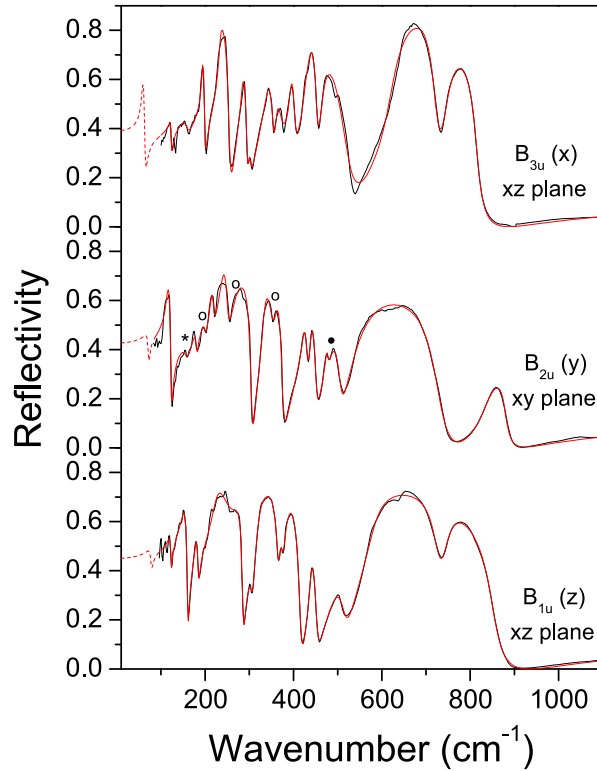


Figure 2. Experimental (black line) and fitting curves (red lines) of the polarized infrared reflectivity spectra of the orthorhombic CaTa_2O_6 single crystal fibre, for the x , y and z polarizations, as indicated. The spectra were obtained for oriented single domains (around $200 \mu\text{m}$ wide). The lowest-frequency modes (indicated by dashed red line) were added to each calculated spectra to improve the fit quality. The TO frequency of these modes are below our measuring range, being taken from Repelin *et al* [18]. For the y -direction, an asterisk and open circles indicate polarization leaks and the closed circle is likely a defect mode.

The polarized spectra in the whole far-mid infrared range were obtained with the light electric field (E) parallel to the three mutually orthogonal crystallographic axes of the orthorhombic *aeschnite* structure. The experimental data for these orthogonal symmetries are presented in figure 2 (black lines), along with the adjusted curves (solid red lines) obtained as discussed below.

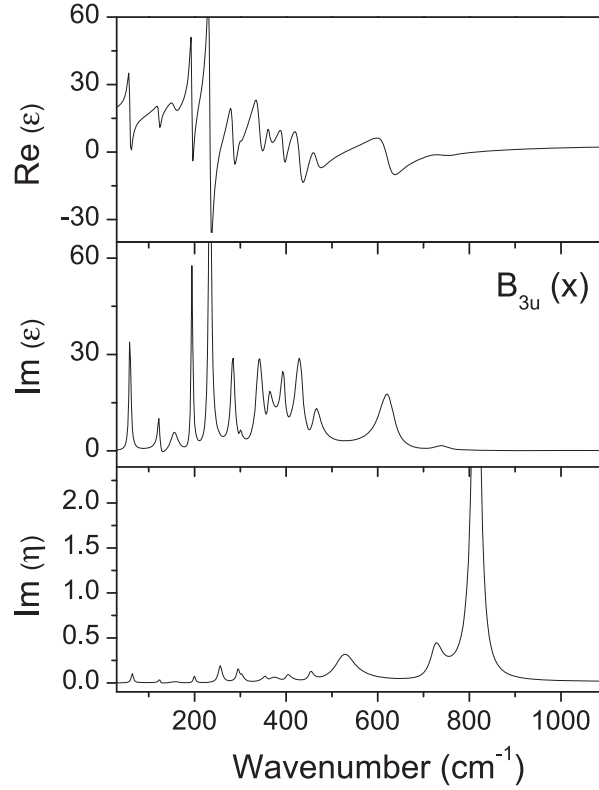
The polarized infrared spectra of figure 2 were fitted by a non-linear least-square program [20], within the four-parameter semi-quantum model [21]. In this framework, at low incidence angles, the infrared reflectivity for each principal direction is given by the Fresnel law:

$$R = \left| \frac{\sqrt{\varepsilon(\omega)} - 1}{\sqrt{\varepsilon(\omega)} + 1} \right|^2, \quad (1)$$

where the complex dielectric dispersion function $\varepsilon(\omega)$, at a wavenumber ω , is given by the contribution of N polar phonons in the chosen direction (*via* the factorized form [21]):

Table 1. Polarization-resolved Raman modes for the orthorhombic CaTa_2O_6 crystal fibre. Peak positions (phonon wavenumbers) are in cm^{-1} .

Parallel configuration A_g type	88, 151, 167, 175, 236, 243, 285, 342, 475, 556, 632, 654, 690
Cross-polarized configuration B_g type ($B_{1g} \oplus B_{2g} \oplus B_{3g}$)	56, 62, 95, 119, 214, 261, 272, 290, 326, 370, 378, 394, 415, 454, 495, 534, 885

**Figure 3.** Optical functions obtained from the fitting of the infrared spectra of the orthorhombic CaTa_2O_6 single crystal fibre, for $E//x$, by the four-parameter semi-quantum model. Top and middle panels present the real and imaginary part of the dielectric function; the bottom panel presents the imaginary part of the reciprocal dielectric constant.

$$\varepsilon(\omega) = \varepsilon_{\infty} \prod_{j=1}^N \frac{\Omega_{j,LO}^2 - \omega^2 + i\omega\gamma_{j,LO}}{\Omega_{j,TO}^2 - \omega^2 + i\omega\gamma_{j,TO}}. \quad (2)$$

In the above expression, ε_{∞} is the electronic polarization contribution, Ω is the frequency and γ the damping of the transverse (TO) or longitudinal (LO) phonon branches.

The solid red curves in figure 2 were obtained after fitting the experimental reflectivity data of our crystal fibre with equations (1) and (2), for each polarization direction. The optical functions obtained from those fittings are presented in figures 3 ($E//x$), 4 ($E//y$) and 5 ($E//z$). The identification of the crystallographic axes is discussed below. In those figures, the top and

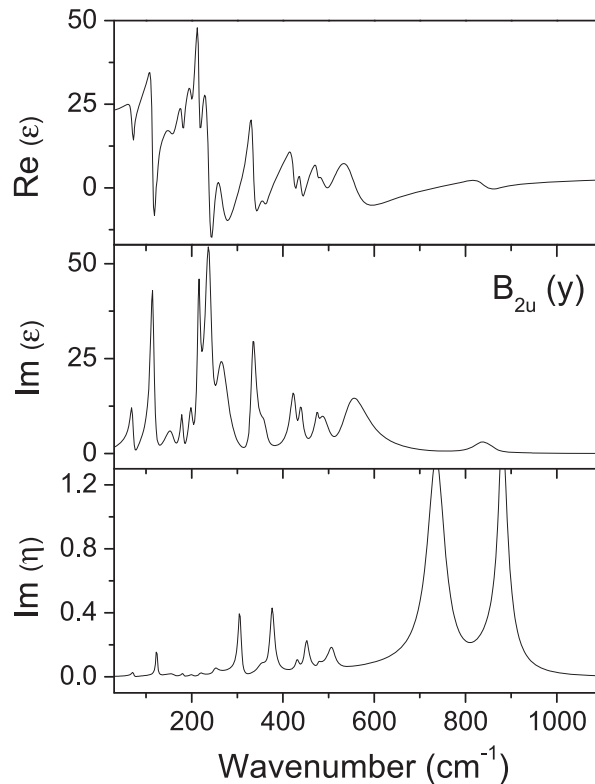


Figure 4. The optical functions (real and imaginary parts of the dielectric constant, imaginary part of the reciprocal dielectric constant) obtained from the fitting of the infrared spectra of the orthorhombic CaTa_2O_6 single crystal fibre, for $E//y$.

middle panels present the real and imaginary part of the dielectric function (ϵ), while the bottom panels present the imaginary part of the reciprocal dielectric constant ($\eta = \epsilon^{-1}$), for each direction. The TO and LO branches of each polar mode, which are the poles and zeros of $\text{Re}(\epsilon)$, are clearly seen in the top panels of figures 3, 4 and 5. Actually, the phonon positions and widths are more accurately determined from the peaks in $\text{Im}(\epsilon)$ and $\text{Im}(\eta)$, for the TO and LO branches, respectively. A visual inspection of figures 3–5 shows us 14 features for $E//x$ and $E//z$, and 16 features for $E//y$ spectra, respectively.

The obtained dispersion parameters for the TO and LO infrared branches are summarized in table 2. The crystallographic directions were determined by comparing the obtained TO phonon frequencies with those proposed by Repelin *et al* based upon lattice dynamic calculations [18]. The agreement between our experimental values and the calculated ones is very good (average deviations for the main bands smaller than 4%). It is worth mentioning that large orthorhombic xz -domains were found in the fibre cross section. Indeed, the growth habit of the fibre favored the y -axis to appear along the fibre axis (a former cubic edge), leading to the appearance of 90° domains in the fibre cross section (xz and zx). Also, the growth facets containing both [001] and [110] cubic directions favored the appearance of xy and yz 90° -orthorhombic domains in this particular longitudinal section. This domain pattern can be understood by the jump of the different lattice parameters at the structural change: a large contraction of the b axis (*ca.* 3%), along with a nearly 45° -rotation of the a (accompanied by a 1.2% expansion) and c axes (contraction of 1.8%) during the cubic to orthorhombic

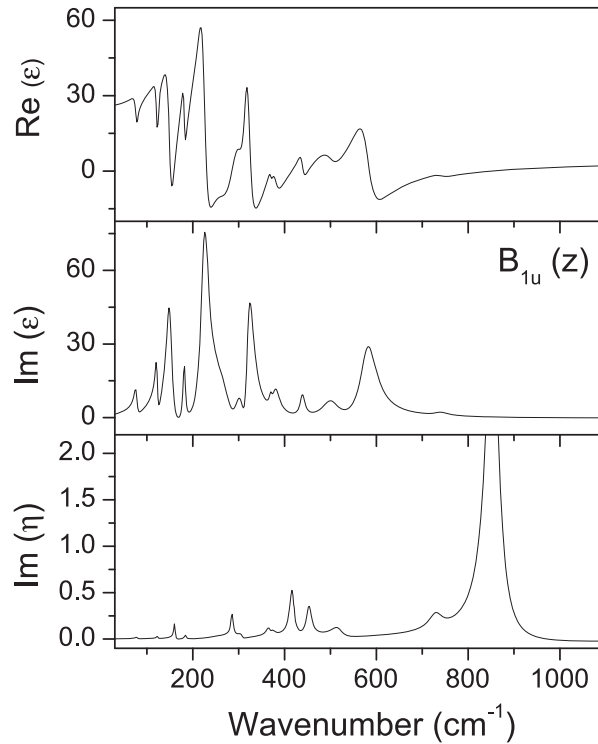


Figure 5. The optical functions (real and imaginary parts of the dielectric constant, imaginary part of the reciprocal dielectric constant) obtained from the fitting of the infrared spectra of the orthorhombic CaTa_2O_6 single crystal fibre, for $E//z$.

transformation. Therefore, thermal stresses during the polymorphic transformation are reduced when the orthorhombic a and c axes appear in the crystal facets, while b tends to be parallel to the crystal fibre—although we also observed less frequent domains with a or c axes in that longitudinal direction.

Now, let us analyze the results of table 2. For x and z polarizations, the spectra of figure 2 were fitted with 14 modes of very good quality. Indeed, the lowest frequency modes were not experimentally discerned. So we added one low-frequency mode for each polarization (dashed red lines in figure 2, for each spectrum), using the TO frequency of Repelin *et al* [18]. Therefore, we believe that table 2 gives the correct (and complete) set of polar phonons along the orthorhombic x and z axes. Concerning the y polarization, five extra features appeared in the spectrum of figure 2, which are listed in table 2 beside the depicted phonon modes. They received symbols, as follows: a star denotes a $\text{LO}(z)$ leak around 160 cm^{-1} ; open diamonds indicate $\text{LO}(x)$ leaks around 200 , 263 and 360 cm^{-1} ; and a closed circle around 476 cm^{-1} is likely a defect mode of unidentified origin. The LO leaks appear as dips in the reflectivity spectra because the p-polarized light carries an electric field component that is normal to the sample surface (this effect occurs because the incident light is not exactly normal to the surface of the sample). This electric field component can excite LO modes whose polarization is normal to the sample interface, leading to dips in the reflectivity spectra, mainly in regions of high reflectivity [22]. The fact that we have dips from $\text{LO}(x)$ and $\text{LO}(z)$ shows that although the y -direction is well oriented, the measuring plane for this spectrum is a mixture of xy and yz planes (due to a mixture of such domains). Once we have identified the extra features in the y -

Table 2. Dispersion parameters from the four-parameters semi-quantum model adjust of the polarized infrared reflectivity spectra of orthorhombic CaTa_2O_6 micro fibres. The wavenumbers (Ω) and damping constants (γ) are in cm^{-1} .

Mode	$\Omega_{j,\text{TO}}$	$\gamma_{j,\text{TO}}$	$\Omega_{j,\text{LO}}$	$\gamma_{j,\text{LO}}$	$\Delta\epsilon_j$	$10^8 \tan \delta_j / \omega$
1	59.0	4.9	64.1	5.2	2.996	22 384
2	122.9	5.5	124.2	3.8	0.405	789
3	156.0	19.3	159.0	18.9	0.787	3318
4	194.2	4.2	199.5	5.1	1.256	742
5	233.6	6.7	256.0	10.2	3.222	2117
6	283.8	10.3	295.8	6.8	1.027	699
7	299.6	6.8	302.0	10.8	0.057	23
8	341.0	18.1	355.8	10.9	1.458	1210
9	361.7	11.8	372.3	35.3	0.270	129
10	394.2	11.3	402.5	14.2	0.442	171
11	430.4	20.7	453.5	13.1	1.326	791
12	464.1	22.9	526.5	54.1	0.532	301
13	623.0	40.4	725.2	31.5	1.149	636
14	739.1	37.7	815.5	18.9	0.073	27
14 $\text{B}_{3u}(x\text{-axis}): \epsilon_\infty = 3.79, \epsilon_r = 18.8,$ $Q_u \times f = 90 \text{ THz}$					$\Sigma \tan \delta_j / \omega = 33\,337 \times 10^{-8}$	
1	70.9	8.0	72.0	5.0	0.768	5367
2	114.9	9.7	123.2	4.0	3.384	10 935
3*	159.0	25.3	160.0	18.1	0.302	1331
4	180.0	7.3	181.0	5.2	0.315	310
5°	200.0	10.4	201.0	8.1	0.386	440
6	215.5	7.4	218.8	8.9	1.288	906
7	238.7	18.5	250.8	13.0	4.112	5881
8°	263.3	38.1	305.8	8.1	3.113	7517
9	333.6	13.4	353.5	23.4	1.112	588
10°	360.0	18.2	376.1	11.4	0.219	135
11	424.7	16.7	431.2	9.1	0.529	215
12	438.8	14.1	451.4	12.1	0.369	119
13•	475.7	7.4	476.9	7.7	0.102	15
14	488.5	42.1	507.2	20.5	0.793	615
15	543.9	72.0	735.3	43.4	1.691	1809
16	832.3	60.0	878.2	16.5	0.149	57
11 $\text{B}_{2u}(y\text{-axis}): \epsilon_\infty = 4.11, \epsilon_r = 22.7,$ $Q_u \times f = 83 \text{ THz}$					$\Sigma \tan \delta_j / \omega = 36\,239 \times 10^{-8}$	
1	77.0	8.0	78.0	6.0	0.745	3880
2	122.1	6.0	123.2	3.5	0.648	1007
3	150.4	15.6	160.7	4.0	4.268	11 384
4	181.4	6.3	184.2	5.2	0.787	583
5	224.9	21.1	248.7	60.9	5.433	8777
6	277.7	55.7	285.7	6.6	1.347	3772
7	305.4	30.8	307.3	10.3	0.592	757
8	320.5	18.6	366.5	12.4	4.066	2855
9	369.9	7.4	372.6	11.2	0.067	14

Table 2. (Continued).

Mode	$\Omega_{j,TO}$	$\gamma_{j,TO}$	$\Omega_{j,LO}$	$\gamma_{j,LO}$	$\Delta\epsilon_j$	$10^8 \tan \delta_j / \omega$
10	379.8	19.2	416.5	12.2	0.492	254
11	438.9	12.9	453.1	13.9	0.267	69
12	501.2	45.8	517.7	29.5	0.589	416
13	580.0	43.9	730.4	36.5	2.246	1136
14	739.3	37.4	854.0	35.2	0.065	17
14 B _{1u} (z-axis): $\epsilon_\infty = 4.17$, $\epsilon_r = 25.8$, Q _u × f = 86 THz					$\Sigma \tan \delta_j / \omega = 34\,922 \times 10^{-8}$	

(*) and (°) are dips from the LO(z) and LO(x) modes, respectively, and (•) is a defect mode.

direction, we have also added a lowest frequency mode for fitting procedures. The final result is that the 11 predicted polar phonon modes for this polarization are also presented in table 2.

By considering tables 1 and 2 together, we can see that, besides obeying their individual symmetries, the selection rules between Raman and infrared modes for this centro-symmetrical system hold perfectly, *i.e.*, no *gerade* mode was seen in the infrared spectra and, conversely, no *ungerade* mode was activated in the Raman spectra of orthorhombic CaTa₂O₆. This result confirms the good quality of our fibres, since defects usually break the selection rules.

At our knowledge, the results presented here constitute the first experimental determination of the polarized phonon spectra of a crystalline material with the *aeschnyite* structure. Therefore, it is important to obtain more quantitative information that can be useful for designed applications of such materials. In particular, the dielectric intrinsic properties can be determined from the polar phonon characteristics of table 2. Indeed, the dielectric strengths of the individual *j*th TO modes (presented in table 2), can be obtained, for each polarization direction, by the equation:

$$\Delta\epsilon_j = \frac{\epsilon_\infty}{\Omega_{j,TO}^2} \times \frac{\prod_k (\Omega_{k,LO}^2 - \Omega_{j,TO}^2)}{\prod_{k \neq j} (\Omega_{k,TO}^2 - \Omega_{j,TO}^2)}. \quad (3)$$

The ‘static’ dielectric constant at the microwave limit ($\Omega_{j,TO} \gg \omega$) is obtained by adding up the core contribution (ϵ_∞) with all the dielectric strengths of same symmetry:

$$\epsilon_r = \epsilon_\infty + \sum_{j=i}^N \Delta\epsilon_j. \quad (4)$$

The calculated ϵ_r and ϵ_∞ values for the orthorhombic CaTa₂O₆ fibres, for each polarization direction, are also presented in table 2. From the adjusted ϵ_∞ values, we can estimate the refractive indices ($\epsilon_\infty = n^2$), as 1.95, 2.03 and 2.04 for the *x*, *y* and *z* axes, respectively, which are quite close to the values obtained for cubic CaTa₂O₆ ($n = 2.01$ [9]) and for an orthorhombic *columbite* CaNb₂O₆ crystal ($1.97 < n < 2.22$ [17]). Concerning the ϵ_r values, by averaging over the three polarization directions, we obtain $\langle \epsilon_r \rangle = 22.4$, which is smaller than the value found for the cubic polymorph (31.7), but comparable with values determined by direct MW measurements in CaTa₂O₆ ceramic samples: 21.2 [1] or 28.3 [2]. The decreasing of ϵ_r after the polymorphic transformation can be a consequence of the increasing covalent character of Ta-O bonds, because of the strong unit cell contraction, as has been observed in RETiTaO₆ (RE = rare

earth) ceramics with *aeschnite* and *columbite* structures [23]. On the other hand, ceramic samples usually have slightly higher dielectric constants than crystals in the MW region, owing to extrinsic contributions from domain walls, grain boundaries and polar defects. Therefore, the obtained ϵ_r for our crystal fibre sounds physically reasonable.

The polar phonon dispersion parameters of table 2 allows also estimation of the intrinsic unloaded quality factor Q_u ($=\cotan \delta$) extrapolated to the MW region ($\Omega_{j,TO} \gg \omega$), from [24]:

$$\tan \delta = \sum_j \tan \delta_j = \sum_j \omega \frac{\Delta \epsilon_j \gamma_{j,TO}}{\epsilon_r \Omega_{j,TO}^2}. \quad (5)$$

The values of the individual and overall losses ($\tan \delta$) are also presented in table 2, for each polarization direction. By averaging the values obtained for the three polarizations, the depicted polar phonons of the CaTa_2O_6 orthorhombic fibre showed an intrinsic $\langle Q_u \times f \rangle$ of 86×10^3 GHz, which is four times higher than the value obtained for the cubic polymorph (20.5×10^3 GHz [9]). The increase in this value is due to the important decrease on the phonon damping for the orthorhombic transformed sample compared to the cubic ones [9]. Indeed, the intrinsic $Q_u \times f$ value obtained here is quite appropriate for MW applications, and can be compared to direct MW responses of tantalum- and niobium-containing perovskites ($Q_u \times f \sim 150\text{--}300 \times 10^3$ GHz and $100\text{--}150 \times 10^3$ GHz, respectively), in ceramic form [25].

The obtained intrinsic unloaded quality factor for our *aeschnite* sample is relatively higher than the direct MW (extrinsic) value measured for a ceramic sample, $Q_u \times f \sim 30.8 \times 10^3$ GHz [2]. Our result suggests that if the dielectric losses of extrinsic origin (impurities, polar species, microstructural defects, etc) in CaTa_2O_6 ceramics were reduced, this system could show a quite adequate dielectric response for MW application—once for good quality centrosymmetric dielectric materials the phononic contribution draw the dielectric response. On the other hand, the appearance of micro-cracks and loss of transparency of the orthorhombic transformed polymorph prevents the optical applications of this crystal phase in compact lasers or other integrated optical devices.

4. Conclusions

We have investigated the vibrational properties of orthorhombic CaTa_2O_6 single crystal fibres. The fibres were initially obtained in an ordered cubic phase by the LHPG method. A polymorphic transformation to the orthorhombic *aeschnite* structure was subsequently induced by long-time annealing (24 h) at 1200 °C. The appearance of multiple domains and micro-cracks accompanying the polymorphic transformation led to diffuse scattering and depolarization of the scattered light in the visible range, but not in the infrared region. Polarized infrared spectra within the micro-domains (ca 200 μm) allowed us to determine the characteristics of the polar phonons for the orthorhombic CaTa_2O_6 . The obtained phononic (intrinsic) dielectric response, $\langle \epsilon_r \rangle = 22.4$ and $\langle Q_u \times f \rangle = 86 \times 10^3$ GHz, shows the appropriateness of CaTa_2O_6 ceramics for MW applications. Totally symmetric Raman modes could be discerned in the polarized Raman spectra, after re-polishing the rough (cracked) sample surface.

Acknowledgments

This work was partially supported by the Brazilian agencies *Conselho Nacional de Desenvolvimento Científico e Tecnológico* (CNPq), *Fundação de Amparo à Pesquisa do Estado de Minas Gerais* (FAPEMIG), and *Fundação de Amparo à Pesquisa do Estado de São Paulo* (FAPESP).

References

- [1] Lee H J, Kim I T and Hong K S 1997 *Jpn. J. Appl. Phys. Part 2* **36** L1318
- [2] Kan A and Ogawa H 2008 *Jpn. J. Appl. Phys.* **47** 7716
- [3] De Camargo A S S, Ferrari C R, Hernandes A C and Nunes L A O 2004 *J. Phys.: Condens. Matter* **16** 5915
- [4] Ferrari C R, de Camargo A S S, Nunes L A O and Hernandes A C 2004 *J. Crystal Growth* **266** 475
- [5] De Camargo A S S, Ferrari C R, Silva R A, Nunes L A O, Hernandes A C and Andreeta J P 2008 *J. Luminescence* **128** 223
- [6] Janhberg L 1959 *Acta Chem. Scand.* **13** 1248
- [7] Janhberg L 1963 *Acta Chem. Scand.* **17** 2548
- [8] Pivovarova A P, Strakhov V I and Smirnov Y N 1998 *Russian J. Appl. Chem.* **71** 1497
- [9] Teixeira N G, Moreira R L, Lobo R P S M, Andreeta M R B, Hernandes A C and Dias A 2011 *Cryst. Growth Des.* **11** 5567
- [10] Tiedemann P and Müller-Buschbaum H 1984 *Z. Anorg. Allg. Chem.* **516** 201
- [11] Almeida R M, Matinaga F M, Andreeta M R B, Hernandes A C, Dias A and Moreira R L 2013 *Cryst. Growth Des.* **13** 5829
- [12] Pivovarova A P, Strakhov V I and Smirnov Y N 1999 *Inorg. Mater.* **35** 1291
- [13] Zurmuhlen R, Petzelt J, Kamba S, Voitsekhovskii V V, Colla E and Setter N 1995 *J. Appl. Phys.* **77** 5341
- [14] Hernandes A C 1999 *Recent Research Developments in Crystal Growth Research* (Trivandrum: Transworld Research Network) p 123
- [15] Andreeta M R B and Hernandes A C 2010 *Springer Handbook of Crystal Growth* ed G Dhanaraj, K Byrappa, V Prasad and M Dudley (Heidelberg: Springer) p 393
- [16] Hayes W and Loudon R 1978 *Scattering of Light by Crystals* (New York: Wiley-Interscience) 7, p 31
- [17] Teixeira N G, Moreira R L, Andreeta M R B, Hernandes A C and Dias A 2011 *Cryst. Growth Des.* **11** 3472
- [18] Repelin Y, Husson E, Dao N Q and Brusset H 1979 *Spectrochimica Acta* **35A** 1165
- [19] Rousseau D L, Bauman R P and Porto S P S 1981 *J. Raman Spectrosc.* **10** 253
- [20] Meneses D D, Gruener G, Malki M and Echegut P 2005 *J. Non-Cryst. Solids* **351** 124
- [21] Gervais F and Echegut P 1986 *Incommensurate phases in dielectrics* ed R Blinc and A P Levanyuk (Amsterdam: North Holland) p 337
- [22] Duarte J L, Sanjurjo J A and Katiyar R S 1987 *Phys. Rev. B* **36** 3368
- [23] Paschoal C W A, Moreira R L, Surendran K P and Sebastian M T 2005 *J. Mater. Res.* **20** 1164
- [24] Petzelt J and Kamba S 2003 *Mater. Chem. Phys.* **79** 175
- [25] Pullar R C 2009 *J. Am. Ceram. Soc.* **92** 563